Optics Letters

Examining second-harmonic generation of high-order Laguerre–Gaussian modes through a single cylindrical lens

XINYUAN FANG,[1] ZEYU KUANG,[1] PENG CHEN,[1] HAOCHENG YANG,[1] QIAN LI,[1] WEI HU,[1] YANQING LU,[1] YONG ZHANG,[1,*] AND MIN XIAO[1,2]

[1]National Laboratory of Solid State Microstructures, College of Engineering and Applied Sciences and School of Physics, Nanjing University, Nanjing 210093, China
[2]Department of Physics, University of Arkansas, Fayetteville, Arkansas 72701, USA
*Corresponding author: zhangyong@nju.edu.cn

Received 17 August 2017; accepted 26 September 2017; posted 28 September 2017 (Doc. ID 304984); published 24 October 2017

We experimentally investigate the second-harmonic generation of a high-order Laguerre–Gaussian (LG) mode under the quasi-phase-matching (QPM) configuration. First, we introduce a simple method to observe the azimuthal (l) and radial (p) indices of the high-order LG modes. Based on the astigmatic transformation technique, l and p are revealed in the number of dark stripes of the converted pattern in the focal plane. Then, using this efficient method of measurement, we demonstrate in experiments a second-harmonic LG mode with its radial and azimuthal indices being twice those of the inputted fundamental wave through QPM in a periodically poled KTP crystal. Our results provide a feasible way to obtain simultaneously the LG modes with larger radial and azimuthal indices.

OCIS codes: (080.4865) Optical vortices; (190.2620) Harmonic generation and mixing; (160.4330) Nonlinear optical materials.

https://doi.org/10.1364/OL.42.004387

The Laguerre–Gaussian (LG) modes, characterized by the azimuthal index l and radial index p, have a well-defined orbital angular momentum (OAM) of $l\hbar$ per photon [1]. This OAM of a LG beam has been widely employed in optical tweezers [2,3], optical manipulation [4], optical trapping [5], imaging [6], and information processing [7–11]. Recently, LG modes with a non-zero radial index have been demonstrated to possess an apparent advantage over those with only azimuthal index in several areas, such as optical manipulation [12,13] and optical communication [14,15]. Moreover, the mirror of gravitational wave (GW) detectors that use high-order LG modes may be less susceptible to thermal noise because of a wider power distribution than low-order modes [16]. As a result, research interest in the radial LG modes has risen.

To date, there are several ways to produce directly high-order LG beams, such as the Q-plate (QP) [17,18], spatial light modulator (SLM) [19], fork grating [20], metasurface [21], spiral phase plate (SPP) [22], and laser crystal [23,24]. Recently, because of an increasing demand in practical applications for LG beams to be converted to particular working wavelengths, researchers have demonstrated second-harmonic generation (SHG) [25–27], sum-frequency generation [28], third-harmonic generation [29,30], high harmonic generation [31], and spontaneous parametric down conversion [32,33] of LG beams. Whereas the azimuthal index is conserved in most of the nonlinear processes, the radial index can be conserved [32,33] or non-conserved [34–36]. In this Letter, we examine the higher order LG beams achieved in quasi-phase-matching (QPM) SHG in a periodically poled $KTiOPO_4$ (PPKTP) crystal.

The measurement of a LG mode with zero radial index, i.e., an OAM mode, is a vibrant area of research. Generally, for classical light beams, the interference scheme is the most popular. The OAM can be determined by counting the fringes generated in interference patterns produced when light interferes with its own mirror image or a reference beam [37–39]. Moreover, OAM can be analyzed from converted patterns produced after the mode converter using single slits [40], double slits [41], apertures of a special shape [42], cylindrical lenses [43–45], or fork gratings [7]. Recently, a single plasmonic nanohole was used to measure the OAM of an optical beam in a simple nondestructive way [46]. However, little has been reported on the radial index of a high-order LG mode [47]. Distinct from previous detecting methods, such as $\pi/2$ mode converter [48], we first demonstrate a method using a single cylindrical lens to measure l and p, leading to a more compact and efficient experimental setup.

In theory, the field focused by a cylindrical lens of focal length f is obtained by solving the paraxial wave equation for the collimated input beam at $z = 0$:

$$E(x, y) = E_0 e^{-r^2/w^2} e^{-il\varphi}(-1)^p \left(r\sqrt{2}/w\right)^l L_p^l(2r^2/w^2). \quad \textbf{(1)}$$

Here $r = \sqrt{(x^2 + y^2)}$, $\varphi = \arctan(y/x)$, w is the beam waist, l is the azimuthal index, p is the radial index, and L_p^l denotes the generalized Laguerre polynomial of index p and l. After passing the cylindrical lens (transmission function:

$t = \exp(-ik_0 y^2/2f)$), the beam intensity in the focal plane is

$$I(u,v) = |U_f(u,v)|^2 = \left| \frac{e^{i\frac{k}{2f}(u^2+v^2)^2}}{i\lambda f} \iint_{-\infty}^{+\infty} E(x,y) t e^{i\frac{k}{2f}(x^2+y^2)} e^{-i\frac{2\pi}{\lambda f}(xu+yv)} \mathrm{d}x\mathrm{d}y \right|^2, \tag{2}$$

where u and v are the orthogonal coordinates at the focal plane, k is the wave vector, and λ the wavelength of the input beam. The simulation results [Figs. 1(b) and 1(e)] of converted patterns at the focal plane for LG modes with different l and p [Figs. 1(a) and 1(d)] exhibit a two-dimensional array of bright spots. In Fig. 1(b), the dotted lines are drawn to emphasize the dark stripes in between the spots of the pattern. Similar to the $\pi/2$ mode converter, the mode indices l and p satisfy relations $l = m - n$ and $p = \min\{m, n\}$. We find that $l = 2$, $p = 1$ for Fig. 1(b) and $l = 2$, $p = 2$ for Fig. 1(e). Both simulation results confirm the relationship between (l, p) and (m, n). Moreover, we also find that the tilt in the stripe indicates the sign of the azimuthal index. In the focal plane of the cylindrical lens, the converted patterns of the LG modes with $+l$ and $-l$ are mirror symmetric along the vertical direction.

To confirm the feasibility of this detecting method, we obtained the converted patterns experimentally. In the experimental setup, the input light is derived from a 4 mW, 633 nm He–Ne laser. Only a single cylindrical lens and a CCD is needed to identify both radial and azimuthal indices. From Fig. 1(c), the l and p of the incident LG beams are set to 2 and 1, respectively. The converted pattern obtained by the CCD is similar to the corresponding pattern of simulations. Moreover, the experimental results for LG_{22} [Fig. 1(f)] also agree well with the simulated pattern in Fig. 1(e).

Next, we use this detection method to demonstrate the conversion of the radial index in the SHG process. The setup proposed to detect the radial index of the SH beams (Fig. 2) uses a fundamental wave (FW) field generated by an optical parametric oscillator (Horizon I-8572, Continuum Co.), which is pumped by a nanosecond laser system with a pulse width of about 6 ns and a repetition rate of 10 Hz. The wavelength can be tuned from 400 nm to 2700 nm. In our experiment, the input wavelength is set at 1064 nm, and the sample used is a periodically poled $KTiOPO_4$ (PPKTP) crystal of the size 10 mm(x) × 5 mm(y) × 0.5 mm(z). The period of the structure is $d = 8.95$ μm. Here, the radial LG modes—those with non-zero radial index—are generated by meta-QPs with radial dislocations that act as half-wave plates with space-varying optical axes and fabricated by photo-patterning birefringent liquid crystals. In our setup, the first quarter wave plate (QWP) changes the polarization of the input laser from linear to circular. After passing the Q-plate, another QWP transforms the polarization of the generated LG beam into linear polarization along the z axis. With this configuration, the nonlinear optical coefficient d_{33} is involved, which is modulated in the PPKTP crystal. After the fundamental beam is filtered out, the SH beams pass the cylindrical lens, and the CCD records the corresponding converted pattern.

For explicitness, we denote the state of the photon of the fundamental beam by $|\vec{k}_1; l_1, p_1>$ with wave vector $\vec{k}_1$, azimuthal index l_1, and radial index p_1 [49]. The SHG process is expressible as

$$|\vec{k}_1; l_1, p_1 > + |\vec{k}_1; l_1, p_1 > \rightarrow |\vec{k}_2; l_2, p_2 > . \tag{3}$$

Here, $\vec{k}_2$ and l_2 are the wave vector and azimuthal index, respectively, of the SH beam, with p_2 its radial index. The OAM conservation law and the phase matching condition require

$$2\vec{k}_1 + \vec{G}_1 = \vec{k}_2 \quad 2l_1 = l_2, \tag{4}$$

where $\vec{G}_1 = 2\pi/d$ is the reciprocal lattice vector generated by the PPKTP.

From the experimental images recorded by the CCD (Fig. 3), we first note that the FW is imprinted with $l_1 = 1$, $p_1 = 1$. The observed FW and SH intensity patterns [Figs. 3(a) and 3(c)] both feature distributions with multiple rings, their number being 2 and 3, respectively. After passing the cylindrical lens, the converted patterns of the FW and SH [Figs. 3(b) and 3(d)] are quite different. As introduced above, by counting the dark stripes in the converted patterns, the radial and azimuthal indices of the SH are both 2 [Fig. 3(d)]. It should be noted that the number of the rings may also indicate the radial index of the LG modes. For example, three rings normally indicate $p = 2$. However, the low intensity of the outer ring of the SH signal in our experiment [Fig. 3(c)] may lead to a misreading of the ring number. If using the single cylindrical lens method, the converted pattern presents clearer results, which makes it a better method in the determination of the

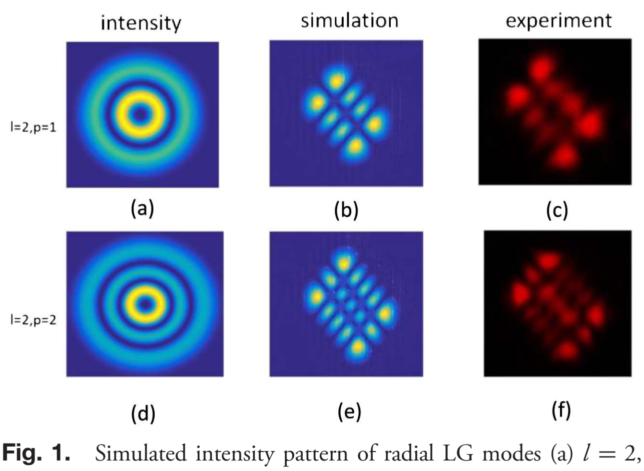

Fig. 1. Simulated intensity pattern of radial LG modes (a) $l = 2$, $p = 1$ and (d) $l = 2$, $p = 2$. Converted patterns of radial LG modes obtained from (b), (e) simulation and (c), (f) experiment.

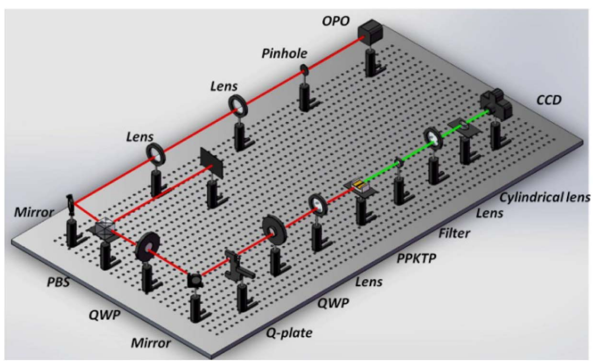

Fig. 2. Schematic of the experimental setup. PBS, polarized beam splitter; QWP, quarter wave plate.

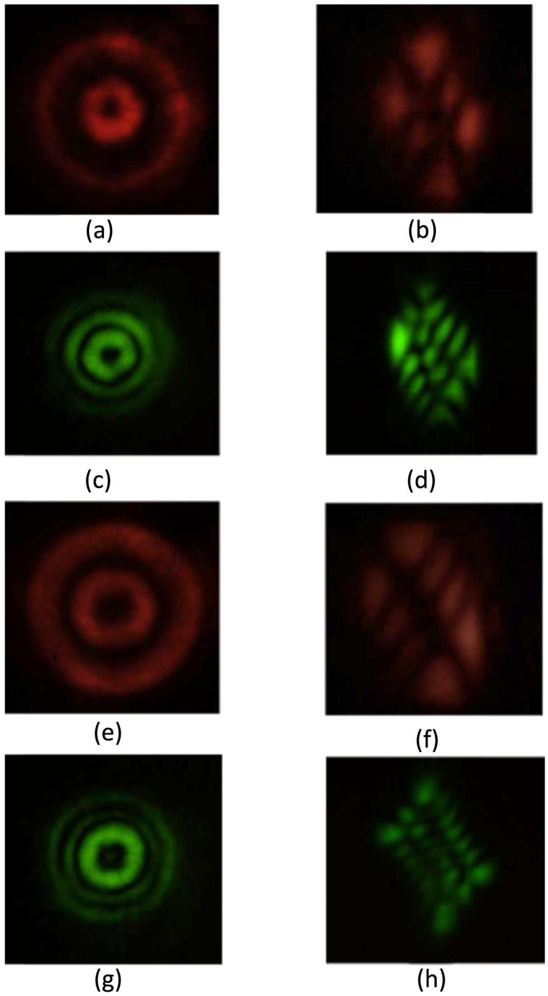

Fig. 3. Intensity and converted patterns of FW (red) and SH (green). The nonlinear processes are (a)–(d) $|\vec{k}_1; 1, 1 > + |\vec{k}_1; 1, 1 > \rightarrow |\vec{k}_2; 2, 2 >$ and (e)–(h) $|\vec{k}_1; 2, 1 > + |\vec{k}_1; 2, 1 > \rightarrow |\vec{k}_2; 4, 2 >$.

radial index under such kind of circumstance. To further test the radial index conversion in the QPM SHG process, we changed the input azimuthal and radial indices to $l_1 = 2$ and $p_1 = 1$ [Figs. 3(e) and 3(f)]. The l and p of the corresponding SH beams are then 4 and 2, respectively [Figs. 3(g) and 3(h)].

When we tune for $l_1 = 1$ and $p_1 = 2$ [Fig. 4(a)], the SH LG modes with $l_2 = 2$ and $p_2 = 4$ are obtained [Fig. 4(b)]. Compared with the well-defined patterns in Figs. 3(d) and 3(h), the imperfect quality of the converted pattern in Fig. 4(d) may be caused by the relatively low purity of the FW with a high radial index [22]. Nevertheless, from this converted pattern, we conclude that with our setup, LG modes with radial index twice that of the FW dominate the SH, which means the radial index is conserved in the QPM SHG process. The experimental results are consistent with previous theoretical predictions [35].

In conclusion, we have demonstrated a simple method using a single cylindrical lens to determine the radial index of the radial LG modes with non-zero p. The results of simulation are consistent with the experimental results. Moreover, we have applied this method to analyze the radial index conversion in the QPM SHG process. The radial index of the SH beams was twice that of the FW. Therefore, the nonlinear optics method presented here can be used to generate higher order LG modes of different frequencies. The increase in the degrees of freedom for light beams, i.e., azimuthal index, radial index, and wavelength, will lead to possible applications in optical communications.

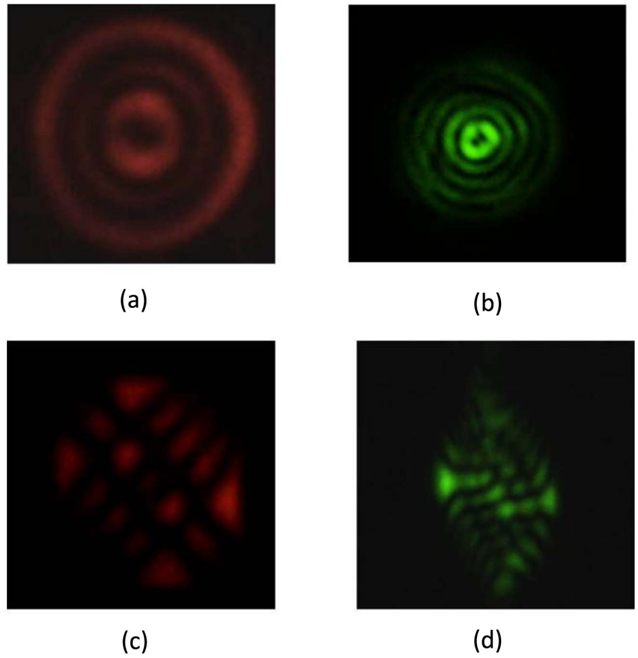

Fig. 4. Intensity and converted patterns of FW (red) and SH (green). The nonlinear process is $|\vec{k}_1; 1, 2 > + |\vec{k}_1; 1, 2 > \rightarrow |\vec{k}_2; 2, 4 >$.

Funding. National Key R&D Program of China (2016YFA0302500, 2017YFA0303700); National Natural Science Foundation of China (NSFC) (11621091, 61490714, 91636106).

REFERENCES

1. L. Allen, M. W. Beijersbergen, R. J. C. Spreeuw, and J. P. Woerdman, Phys. Rev. A **45**, 8185 (1992).
2. D. G. Grier, Nature **424**, 810 (2003).
3. S. Tao, X. C. Yuan, J. Lin, X. Peng, and H. Niu, Opt. Express **13**, 7726 (2005).
4. J. R. Collins and A. Stuart, J. Opt. Soc. Am. **60**, 1168 (1970).
5. M. P. MacDonald, L. Paterson, K. Volke-Sepulveda, J. Arlt, W. Sibbett, and K. Dholakia, Science **296**, 1101 (2002).
6. S. Barnet, A. Jesacher, S. Furhapter, C. Maurer, and M. Ritsch-Marte, Opt. Express **14**, 3792 (2006).
7. A. Mair, A. Vaziri, G. Weihs, and A. Zeilinger, Nature **412**, 313 (2001).
8. A. C. Dada, J. Leach, G. S. Buller, M. J. Padgett, and E. Andersson, Nat. Phys. **7**, 677 (2011).
9. J. T. Barreiro, T. C. Wei, and P. G. B. Kwiat, Nat. Phys. **4**, 282 (2008).
10. D. S. Ding, Z. Y. Zhou, B. S. Shi, and G. C. Guo, Nat. Commun. **4**, 2527 (2013).
11. G. Molina-Terriza, J. P. Torres, and L. Torner, Nat. Phys. **3**, 305 (2007).
12. S. A. Kennedy, M. J. Szabo, H. Teslow, J. Z. Porterfield, and E. R. I. Abraham, Phys. Rev. A. **66**, 043801 (2002).

13. J. Arlt, T. Hitomi, and K. Dholakia, Appl. Phys. B **71**, 549 (2000).
14. A. Trichili, C. Rosales-Guzman, A. Dudley, B. Ndagano, A. B. Salem, M. Zghal, and A. Forbes, Sci. Rep. **6**, 27674 (2016).
15. G. Xie, Y. Ren, Y. Yan, H. Huang, N. Ahmed, L. Li, Z. Zhao, C. Bao, M. Tur, S. Ashrafi, and A. Willner, Opt. Lett. **41**, 3447 (2016).
16. M. Granata, C. Buy, R. Ward, and M. Barsuglia, Phys. Rev. Lett. **105**, 231102 (2010).
17. L. Marrucci, C. Manzo, and D. Paparo, Phys. Rev. Lett. **96**, 163905 (2006).
18. W. Ji, C. H. Lee, P. Chen, W. Hu, Y. Ming, L. Zhang, T. H. Lin, V. Chigrinov, and Y. Q. Lu, Sci. Rep. **6**, 25528 (2016).
19. Y. Ohtake, T. Ando, N. Fukuchi, N. Matsumoto, H. Ito, and T. Hara, Opt. Lett. **32**, 1411 (2007).
20. P. Chen, S. J. Ge, L. L. Ma, W. Hu, V. Chigrinov, and Y. Q. Lu, Phys. Rev. Appl. **5**, 044009 (2016).
21. Y. Wang, X. Fang, Z. Kuang, H. Wang, D. Wei, Y. Liang, Q. J. Wang, T. Xu, Y. Zhang, and M. Xiao, Opt. Lett. **42**, 2463 (2017).
22. G. Ruffato, M. Massari, and F. Romanato, Opt. Lett. **39**, 5094 (2014).
23. H. Yu, M. Xu, Y. Zhao, Y. Wang, S. Han, H. Zhang, Z. Wang, and J. Wang, AIP Adv. **3**, 092129 (2013).
24. Y. Zhao, Z. Wang, H. Yu, S. Zhuang, H. Zhang, X. Xu, J. Xu, X. Xu, and J. Wang, Appl. Phys. Lett. **101**, 031113 (2012).
25. K. Dholakia, N. B. Simpson, M. J. Padgett, and L. Allen, Phys. Rev. A **54**, R3742 (1996).
26. X. Y. Fang, D. Z. Wei, D. M. Liu, W. H. Zhong, R. Ni, Z. H. Chen, X. P. Hu, Y. Zhang, S. N. Zhu, and M. Xiao, Appl. Phys. Lett. **107**, 161102 (2015).
27. Y. Wang, D. Wei, Y. Zhu, H. Huang, X. Fang, W. Zhong, Q. Wang, Y. Zhang, and M. Xiao, Appl. Phys. Lett. **109**, 081105 (2016).
28. Y. Li, Z. Zhou, D. Ding, and B. Shi, J. Opt. Soc. Am. B **32**, 407 (2015).
29. X. Fang, G. Yang, D. Wei, D. Wei, R. Ni, W. Ji, Y. Zhang, X. Hu, W. Hu, Y. Lu, S. Zhu, and M. Xiao, Opt. Lett. **41**, 1169 (2016).
30. D. Wei, J. Guo, X. Fang, D. Wei, R. Ni, P. Chen, X. P. Hu, Y. Zhang, W. Hu, Y. Q. Lu, S. N. Zhu, and M. Xiao, Opt. Express **25**, 11556 (2017).
31. G. Gariepy, J. Leach, K. T. Kim, T. J. Hammond, E. Frumker, R. W. Boyd, and P. B. Corkum, Phys. Rev. Lett. **113**, 153901 (2014).
32. H. H. Arnaut and G. A. Barbosa, Phys. Rev. Lett. **85**, 286 (2000).
33. S. Feng and P. Kumar, Phys. Rev. Lett. **101**, 149303 (2009).
34. J. Courtial, K. Dholakia, L. Allen, and M. J. Padgett, Phys. Rev. A **56**, 4193 (1997).
35. G. H. Shao, Z. J. Wu, J. H. Chen, F. Xu, and Y. Q. Lu, Phys. Rev. A **88**, 063827 (2013).
36. Z. H. Zhu, W. Gao, C. Y. Mu, and H. W. Li, Optica **3**, 212 (2016).
37. M. Padgett, J. Arlt, N. Simpson, and L. Allen, Am. J. Phys. **64**, 77 (1996).
38. J. Leach, M. J. Padgett, S. M. Barnett, S. Franke-Arnold, and J. Courtial, Phys. Rev. Lett. **88**, 257901 (2002).
39. J. A. Huguenin, B. Coutinho dos Santos, P. A. dos Santos, and A. Z. Khoury, J. Opt. Soc. Am. A **20**, 1883 (2003).
40. D. P. Ghai, P. Senthikumaran, and R. S. Sirohi, Opt. Laser Eng. **47**, 123 (2009).
41. H. I. Sztul and R. R. Alfano, Opt. Lett. **31**, 999 (2006).
42. J. M. Hiclmann, E. J. S. Fonseca, W. C. Soares, and S. Chavez-Cerda, Phys. Rev. Lett. **105**, 053904 (2010).
43. V. Denisenko, V. Shvedov, A. S. Desyatnikov, D. N. Neshev, W. Krolikowski, A. Volyar, M. Sokin, and Y. S. Kivshar, Opt. Express **17**, 23374 (2009).
44. S. Li, L. Kong, Z. Ren, Y. Li, C. Tu, and H. Wang, Phys. Rev. A **88**, 035801 (2013).
45. Y. Zhang, H. Yu, H. Zhang, X. Xu, J. Xu, and J. Wang, Opt. Express **24**, 5514 (2016).
46. D. Wei, Y. Wang, D. Liu, Y. Zhu, W. Zhong, X. Fang, Y. Zhang, and M. Xiao, ACS Photon. **4**, 996 (2017).
47. B. Sephoton, A. Dudley, and A. Forbes, Appl. Opt. **55**, 7830 (2016).
48. J. Zhou, W. Zhang, and L. Chen, Appl. Phys. Lett. **108**, 111108 (2016).
49. J. Harris, V. Grillo, E. Mafakheri, G. C. Gazzadi, S. Frabboni, R. W. Boyd, and E. Karimi, Nat. Phys. **11**, 629 (2015).